HHS Public Access

Author manuscript

Nat Photonics. Author manuscript; available in PMC 2018 September 26.

Published in final edited form as:

Nat Photonics. 2018 April ; 12(4): 195–201. doi:10.1038/s41566-018-0134-3.

Opto-thermoelectric nanotweezers

Linhan Lin[1,2,†], **Mingsong Wang**[1,†], **Xiaolei Peng**[2,†], **Emanuel N. Lissek**[3], **Zhangming Mao**[4], **Leonardo Scarabelli**[5,6], **Emily Adkins**[7], **Sahin Coskun**[8], **Husnu Emrah Unalan**[8], **Brian A. Korgel**[7], **Luis M. Liz-Marzán**[5,9,10], **Ernst-Ludwig Florin**[3], and **Yuebing Zheng**[1,2,*]

[1]Department of Mechanical Engineering, The University of Texas at Austin, Austin, TX 78712, USA

[2]Materials Science & Engineering Program and Texas Materials Institute, The University of Texas at Austin, Austin, TX 78712, USA

[3]Center for Nonlinear Dynamics, Department of Physics, The University of Texas at Austin, Austin, TX 78712, USA

[4]Department of Engineering Science and Mechanics, The Pennsylvania State University, University Park, PA 16802, USA

[5]Bionanoplasmonics Laboratory, CIC biomaGUNE, Paseo de Miramón 182, 20014 Donostia-San Sebastián, Spain

[6]California NanoSystems Institute, University of California, Los Angeles, Los Angeles, California 90095, United States

[7]Department of Chemical Engineering, The University of Texas at Austin, Austin, TX 78712, USA

[8]Department of Metallurgical and Materials Engineering, Middle East Technical University, Ankara 06800, Turkey

[9]Ikerbasque, Basque Foundation for Science, 48013 Bilbao, Spain

[10]CIBER de Bioingeniería, Biomateriales y Nanomedicina, CIBER-BBN, 20014 Donostia-San Sebastián, Spain

Abstract

Optical manipulation of plasmonic nanoparticles provides opportunities for fundamental and technical innovation in nanophotonics. Optical heating arising from the photon-to-phonon

Correspondence and requests for materials should be addressed to Y.Z. (zheng@austin.utexas.edu).

†These authors contributed equally to this work.

Author contributions: L.L. and Y.Z. conceived the idea. L.L., M.W. X.P. prepared the materials, worked on the trapping experiments, and collected the data. E.N.L., X.P., and E.-L.F. worked on the measurements of trapping stiffness. Z.M. conducted the CFD simulations. L.L. conducted FDTD simulations. L.S. and L.M.L.-M. synthesized the AuNTs. E.A., S.C., H.E.U. and B.A.K. synthesized the AgNWs. Y.Z. supervised the project. All authors participated in the discussions of the results and wrote the manuscript.

Supplementary information is available in the online version of the paper.

Competing financial interests: The authors declare no competing financial interests.

conversion is considered as an intrinsic loss in metal nanoparticles, which limits their applications. We show here that this drawback can be turned into an advantage, by developing an extremely low-power optical tweezing technique, termed opto-thermoelectric nanotweezers (OTENT). Through optically heating a thermoplasmonic substrate, alight-directed thermoelectric field can be generated due to spatial separation of dissolved ions within the heating laser spot, which allows us to manipulate metal nanoparticles of a wide range of materials, sizes and shapes with single-particle resolution. In combination with dark-field optical imaging, nanoparticles can be selectively trapped and their spectroscopic response can be resolved *in-situ*. With its simple optics, versatile low-power operation, applicability to diverse nanoparticles, and tuneable working wavelength, OTENT will become a powerful tool in colloid science and nanotechnology.

Optical manipulation of plasmonic nanoparticles offers the possibility of dynamic control of light-matter interactions at the nanoscale, which is of interest for various applications in nanophotonics, materials science and life sciences. Optical tweezers have been shown to trap metal nanoparticles in diffraction-limited laser beams with high light intensity, since they provide a sufficient optical gradient force[1]. Although the use of optical tweezers succeeded in trapping Au and Ag nanoparticles with different sizes and shapes[2-8], it typically encounter technical obstacles. First of all, upon excitation of localized surface plasmons (LSPs) at metal nanoparticles by the trapping laser beam, enhanced light absorption and scattering result in optical heating of the particles and strong optical radiation forces, thereby significantly reducing the trapping stability[1,9,10]. As a result, optical trapping is limited to near-infrared lasers with wavelengths far away from the LSP resonance of the metal nanoparticles[3,4,9]. Second, optical tweezers can only trap metal nanoparticles with sizes significantly smaller than the laser wavelength (*i.e.*, in the Rayleigh regime), where the nanoparticle can be treated as a dipole. Optical trapping of metal particles with sizes comparable to, or larger than the laser wavelength, is challenging because the enhanced light-scattering cross-section increases the optical scattering force[1,11]. Finally, high laser power (tens to hundreds of milliwatts) is required to trap subwavelength metal nanoparticles. Such a high optical power can potentially damage the functional materials, surface molecules, or even the trapped metal nanoparticles[12].

Optical trapping of metal nanoparticles with LSPs excited at a low optical power is expected to facilitate *in-situ* optical spectroscopy, leading to insights into plasmon coupling and its applications in sensing, imaging and photothermal therapy. The photothermal effect, or Joule loss, is often recognized as an intrinsic limitation for the use of metal plasmonic nanoparticles in nanophotonic devices[13,14]. But the Joule loss can also be turned into an advantage. It has been demonstrated that the heat generated can benefit optical trapping by creating an electrothermoplasmonic flow that delivers nanoparticles to the trapping site[15]. Optical confinement of single nanoparticles or macromolecules has been achieved *via* a dynamic temperature field[16,17]. However, the particles or molecules in the dynamic temperature field undergo frequent and broad position fluctuations. Thermal convective flow and thermophoresis were also employed to trap dielectric microparticles in the hot regions[18,19]. However, a tweezing platform based on photothermal effects with both low operation power and general applicability is still elusive. More recently, we have proposed a strategy that implements a thermoelectric field to reversibly assemble metal nanoparticles

into clusters[20]. Herein, by exploring nanoparticle migration along a light-controlled thermoelectric field, we developed opto-thermoelectric nanotweezers (OTENT) that allow us to capture and manipulate metal nanoparticles at single-particle resolution.

Working Principle

To enable OTENT, we added a cationic surfactant, cetyltrimethylammonium chloride (CTAC), to the nanoparticle colloid. CTAC molecules adsorb on the particle surface and form a positively charged molecular double layer (Fig. 1a and Supplementary Fig. 1)[21,22]. Simultaneously, CTAC molecules self-assemble into micelles when above the critical micelle concentration (cmc, 0.13-0.16 mM). With high charge density and nanoscale size, CTAC micelles act as macro cations (known as micellar ions, Fig. 1b), which, together with the Cl^- counter-ions (Fig. 1c), provide the thermoelectric field in OTENT.

Without optical heating, both the ions and the metal particles are randomly dispersed in the solution, without a preferred migration direction (Fig. 1d). To generate an optically controllable temperature gradient field, we directed a laser beam to a thermoplasmonic substrate, i.e., a porous Au film which was fabricated by simple deposition of an Au layer followed by thermal annealing (see Supplementary Fig. 2 for substrate geometry and Methods for fabrication procedure). A cross-sectional view of the simulated temperature distribution (embedded in the scheme) at the substrate-solution interface is shown in Fig. 1e. We can see that a temperature difference of ~12 K was obtained when the porous Au film was irradiated by a 532 nm laser beam at an optical power of 0.216 mW and a beam diameter of 2 μm. It should be noted that the CTAC micelles are thermally stable over a wide temperature range, which is broader than the working temperature range in this work[23]. Both the micellar ions and Cl^- ions undergo thermophoresis, migrating from a hot to a cold region (see Supplementary Note 1). At the steady state, the spatial redistribution of both CTAC micelles and Cl^- ions generates an electric field, which is given by[24]

$$E_{\mathrm{T}} = \frac{k_{\mathrm{B}} T \nabla T}{e} \frac{\sum_i Z_i n_i S_{\mathrm{T}i}}{\sum_i Z_i^2 n_i} \quad (1)$$

i indicates the ionic species, i.e. CTAC micellar ions or Cl^- ions, k_{B} is the Boltzmann constant, T is the environmental temperature, ∇T is the temperature gradient, e is the elemental charge, while Z_i, n_i, and $S_{\mathrm{T}i}$ are the charge number, the concentration, and the Soret coefficient of i species, respectively. Since the CTAC micelle has a higher molecular mass and a larger Soret coefficient than the Cl^- ions, i.e. S_{T} (micelle) ~10^{-2} K^{-1} > S_{T} (Cl^-) ~7.18×10^{-4} K^{-1}, we obtain an electric field E_{T} pointing towards the laser beam arising from the spatial redistribution of both the CTAC micelles and the Cl^- ions[20,25], which can trap the positively charged metal nanoparticle at the laser spot, as shown in Fig. 1f. Under a temperature gradient of 0.5-3×10^7 K m^{-1}, we estimate the trapping electric field to be 50-300 V m^{-1}. The corresponding in-plane and out-of-plane temperature gradients and trapping forces $F_{\mathrm{T}}=qE_{\mathrm{T}}$ are schematically presented in Figs. 1g and h, where q is the charge of the metal nanoparticles. This trapping electric field is balanced by the repulsive electric

field, E_T, arising from the positive charge of the thermoplasmonic substrate, which is also coated by the CTAC double layers. Different from optical tweezers, where the particles are trapped by the optical gradient force from a highly focused laser beam, the trapping electric field in OTENT arises from optical heating, which can relax the rigorous optical requirements of optical tweezers.

Single-Nanoparticle Trapping and Manipulation

We first demonstrate the use of OTENT for trapping and manipulating single Au nanospheres (AuNSs) and Ag nanospheres (AgNSs). Due to their strong light scattering at the LSP resonance wavelengths, AuNSs and AgNSs were tracked with *in-situ* dark-field optical imaging. Fig. 2a shows the trapping process of a single 100 nm AgNS using a low-power 532 nm laser beam. The optical intensity we used was 0.05-0.4 mW μm^{-2}, which is 2-3 orders lower than the typical optical intensity in optical tweezers (10-100 mW μm^{-2}). Different from the plasmon-enhanced optical force on plasmonic nanoantennas, which is limited by the decay length of LSPs[15,26], the temperature gradient field has a much larger working range (Figs. 1g and h). Thus, OTENT can effectively deliver the metal nanoparticles to the trapping centre within a surrounding region of 5-10 μm in radius and dynamically transport the trapped particle at will by directing the laser beam. As shown in Fig. 2b, we delivered a trapped AgNS over a distance of ~110 μm in 9 s. Interestingly, the trapped particle was released as soon as the heating laser was turned off and the temperature gradient field disappeared (Fig. 2c, also see Supplementary Movie 1 for real-time trapping, dynamic transport and release process).

To evaluate the trapping stability, we measured the trapping stiffness of OTENT by tracking the Brownian motion of the trapped nanoparticles using a quadrant photodiode (see Methods for details). A low-power laser beam (671 nm, 0.4 mW) was used to trap single metal nanoparticles, including 100 nm AgNSs and 100 nm AuNSs. The measured trapping stiffness ranges from 80 to 2600 fN μm^{-1}. The trapping stiffness is comparable to that of a single 200 nm polystyrene bead trapped by plasmonic Au nanodimers. However, the optical power used in OTENT is 3 orders of magnitude lower than that in the plasmonic tweezers[27]. We also compared the trapping stiffness of OTENT with that of traditional optical tweezers in the trapping of metal nanoparticles. Specifically, for traditional optical tweezers at an optical power of 0.4 mW, optical trapping of a single 100 nm AuNS using a highly focused 1064 nm laser beam has a stiffness of ~2.5 fN μm^{-1}, indicating that the trapping stiffness of OTENT is 2-3 orders of magnitude higher than that of optical tweezers[6].

Furthermore, we can optimize the trapping capability of OTENT by tuning the CTAC concentration that influences the micelle thermophoresis. We have measured the trapping stiffness of 100 nm AgNSs and 100 nm AuNSs at different CTAC concentrations, as summarized in Figs. 2d and e. An increase of surfactant concentration reduces the Soret coefficient of the micelles[28,29] and in turn the electric field intensity, according to equation 1. In Figs. 2d and e, we observe that the trapping stiffness decreases when the CTAC concentration is increased from 0.2 mM to 2 mM, for both 100 nm AgNSs and 100 nm AuNSs. Interestingly, the trapping stability is dramatically improved when the CTAC concentration is further increased. We attribute the improved trapping stability to the

increased substrate-particle interaction driven by depletion of CTAC micelles. The thermophoresis of CTAC micelles, i.e., migration from the hot to the cold regions, causes the depletion of CTAC micelles at the particle-substrate gap. The micelle depletion generates an osmotic pressure exerted on the particle to improve its trapping stability. In addition, the depletion attraction significantly reduces the particle-substrate distance, which increases logarithmically the Soret coefficient of the particle[30]. In OTENT, the opto-thermoelectric field is proportional to the Soret coefficient of the particle, indicating an increased trapping force due to the reduction of the particle-substrate gap. At a CTAC concentration of 20 mM, the trapping stiffness of OTENT for both 100 nm AgNSs and 100 nm AuNSs reaches 1 pN μm^{-1} and even higher despite a low optical power of 0.4 mW. Since the temperature gradient is almost linear at the beam centre, the trapping potential there can be treated as harmonic and the whole trapping potential can be further calculated according to the temperature distribution. Fig. 2f shows the trapping potential of a single 100 nm AgNS in 20 mM CTAC solution, with a trapping depth of 48 $k_B T$. The maximum trapping force reaches 350 fN (Fig. 2g), indicating that a stable trapping of nanoparticles can be achieved at a low optical power. It should be noted that, although the depletion attraction force is not the main driving force to initialize the trapping in OTENT (Supplementary Note 2), it is critically important to improve the trapping stability at high CTAC concentration. At 20 mM, the particle-substrate interaction (including depletion attraction, van der Waals interaction, and electrostatic interaction) becomes dominant, yielding a trapping potential of 24 k_BT for a single 100 nm AuNS (Supplementary Note 3) and reasonably agrees with the measured trapping potential (22.8 k_BT).

In-Situ Optical Spectroscopy

To carry out *in-situ* dark-field optical spectroscopy of the trapped metal nanoparticles, we incorporated a high-performance spectrometer into OTENT, as shown in Fig. 3a. It should be noted that particle-substrate plasmonic coupling can occur when the particles are trapped in the vicinity of the substrate. However, in OTENT, the backward scattering from the porous Au film is very weak and the particle-substrate plasmonic coupling can be ignored, which provides the possibility to detect the intrinsic scattering spectra from the trapped particles. In Fig. 3b, we selectively trapped individual AgNSs according to their scattered colour and recorded the scattering spectra[31]. By matching the experimental spectra with simulated spectra, we verified the sizes of the AgNSs. The colour of AgNSs changes from violet to blue when the diameter increases from 70 nm to 100 nm, with an improved polarizability, a reduced electric field enhancement factor, and a LSP peak red-shift from 440 to 495 nm. The *in-situ* scattering imaging and spectroscopy of single AuNSs of 80-100 nm in diameter are summarized in Fig. 3c. Optical trapping of metal nanoparticles imposes critical requirements on the laser wavelength. For example, it would be challenging to trap AuNSs with a 532 nm laser using optical tweezers, due to the enhanced repulsive optical scattering force by excitation of the LSPs. However, with OTENT we can achieve trapping using lasers with working wavelengths either close to, or far away from the resonance wavelength of the metal nanoparticles (see Supplementary Fig. 3 for the trapping with a 532 nm laser).

The versatility of OTENT was explored by trapping nanoparticles with different morphologies. Shown in Fig. 3d is the trapping of single anisotropic Au nanotriangles (AuNTs) with different side lengths of 140 nm and 60 nm, respectively. It should be noted that the trapped 60 nm AuNT shows a yellow colour, which arises from a mixture of the red light scattered by the AuNT (646 nm) and the fluorescence and scattering light from the thermoplasmonic substrate (Supplementary Fig. 4). We have also achieved stable trapping of single small Au nanorods (AuNRs) without increasing the incident optical power (Fig. 3e). The fluorescence light from the thermoplasmonic substrate dominated over the weak scattered light from the single AuNR, due to its small size. As a result, an overall green colour was observed from the trapped AuNR (Supplementary Fig. 5). Non-luminescent or non-plasmonic substrates with a high absorption coefficient and low thermal conductivity can be used to improve the *in-situ* characterization capability for smaller particles. To further verify that single metal nanoparticles were trapped, we printed the particles on the substrates and checked the samples using scanning electron microscopy (Supplementary Fig. 6). The smallest particles we trapped using low optical power in the current experimental setup were 20 nm AuNSs (Supplementary Fig. 7). It should be noted, while low-power trapping of smaller particles with OTENT is possible, the experimental demonstration of trapping such particles was limited by our capability for *in-situ* spectroscopic analysis of the trapped particles over the thermoplasmonic substrate. With a suitable detection method, we could experimentally push the size limit of trapped particles down to sub-10 nm through substrate optimization or the use of an ultrafast laser. We have also utilized OTENT to trap large metal nanoparticles (*e.g.*, 400 nm AuNSs), however, the upper size limit remains to be tested (Supplementary Note 4). In addition, we also demonstrated that OTENT can be used to manipulate one-dimensional metal nanowires with precise location and orientation control (Supplementary Note 5).

Parallel and Multiple Trapping

The arbitrary light manipulation by means of a digital micromirror device (DMD) allows us to trap and manipulate multiple metal nanoparticles in parallel using OTENT. As shown in Fig. 4a, we created six laser beams with the DMD to capture six 100 nm AgNSs, with one nanosphere in each beam. The successive dark-field optical images show the six AgNSs trapped into a circle pattern (see Supplementary Movie 2 for a real-time movie). As another example, we created and arranged six laser beams into a triangular pattern, where each beam trapped a single 140 nm AuNT (Fig. 4b). It should be noted that the metal nanoparticles trapped in parallel can interact with each other through optical binding[32]. However, considering the low optical power used in OTENT, the optical binding force was limited and did not significantly affect the trapping behaviour. Such a parallel nanoparticle manipulation represents an opportunity for dynamic lithography with single-particle resolution.

We further explored OTENT to trap multiple metal nanoparticles using a single laser beam and to control the particle-particle interactions within the trap. Fig. 4c shows three interaction forces between two trapped particles, including the depletion attractive force F_d, van der Waals force F_{vdw} and electrostatic repulsive force F_e. Assuming that optical heating leads to complete depletion of the CTAC micelles, we calculated the total interaction potential $U_{total} = U_d + U_{vdw} + U_e$, where U_d, U_{vdw}, and U_e are the depletion attraction

potential, van der Waals potential and electrostatic potential, respectively (Fig. 4d). The electrostatic interaction between CTAC micelles and AuNSs was also taken into consideration by treating the CTAC micelles as highly charged depletants (see Supplementary Note 3 for the full derivation of the theoretical model)[33]. We can see that an increase in CTAC concentration leads to a deeper attractive potential with a reduced inter-particle gap, which arises from the increased osmotic imbalance and reduced electrostatic repulsion.

Understanding the interaction potential allows us to tune particle-particle plasmon coupling within the trap[34-36]. As a demonstration, we selected two different CTAC concentrations, 1 mM and 20 mM, to tune the inter-particle gaps between 65 nm and 25 nm (Fig. 4d). We then selectively trapped a single 100 nm AuNS and two 100 nm AuNSs in the 1 mM CTAC solution for *in-situ* optical spectroscopy. As shown in the top and bottom panels of Fig. 4e, increased scattering intensity was observed with no spectral shift when the number of the trapped particles changed from one to two at a single thermal hot spot, revealing that no near-field coupling was achieved between the two 100 nm AuNSs. In contrast, we observed that the single scattering peak for a single trapped AuNS split into two peaks when two AuNSs were trapped in the 20 mM CTAC solution. A yellow spot in the dark-field optical image (mixture of the two scattering peaks) with increased scattering intensity also reveals optical coupling between both AuNSs. To further verify the LSP coupling observed in Fig. 4f, we simulated the scattering spectra and electric field enhancement profiles of a single 100 nm AuNS and a 100 nm AuNS dimer with a gap of 25 nm (Fig. 4g). We can see that the AuNS dimer with near-field coupling exhibits a longitudinal mode at 638 nm and a transverse mode at 568 nm, which are red shifted and blue-shifted, respectively, with respect to the dipole mode at 580 nm for the single 100 nm AuNS. The simulations match well with the experimental spectra in Fig. 4f. This controllable near-field coupling allows us to precisely tune the optical properties of designer colloidal metamaterials.

We further demonstrated *in-situ* monitoring of the trapping dynamics by recording the time-dependent scattering intensity at a specific wavelength. A CTAC concentration of 1 mM was selected to avoid near-field coupling between the trapped particles, and the background from the thermoplasmonic substrate was removed. From Fig. 4h, we can see that, once a single 100 nm AuNS was captured by the thermoelectric field, the scattering intensity at 580 nm increased immediately. The scattering intensity fell back to zero once the particle was released. Without significant near-field coupling between the trapped particles, we can also estimate the number of trapped particles according to the recorded photon counts. As shown in Fig. 4i, the photon counts increased linearly with the number of AuNSs in the trap, which also verifies that no obvious near-field plasmonic coupling occurs between the multiple trapped AuNSs in 1 mM CTAC solution. It should be noted that the trapped particles can further absorb the incident laser power and increase the temperature around the trapping spot (see Supplementary Fig. 8) for improved trapping efficiency.

Conclusions

Through an innovative management of light, heat, and electric field in opto-thermoplasmonic fluidics, we developed OTENT for optical trapping and versatile

manipulation of metal nanoparticles with single-particle resolution, using *in-situ* optical spectroscopy. In addition to their conventional role in surface modification of metal nanoparticles, ionic surfactants were further exploited to act as micellar ions that create light-controlled thermoelectric fields, and as charged depletants to manipulate the interaction between trapped particles. As a general tweezing technique, OTENT is applicable to a wide range of metal, semiconductor, polymer and dielectric nanostructures with charged or hydrophobic surfaces. So far, we have succeeded in trapping silicon nanospheres, silica beads, polystyrene beads, silicon nanowires, germanium nanowires, and metal nanostructures. However, OTENT relies on ionic surfactants in the nanoparticle suspensions to create a thermoelectric field. This requires a solvent environment replacement for nanoparticles that are not dispersed in the ionic surfactants. Challenges may arise for colloidal nanoparticles that cannot be easily modified by surfactants. Additionally, OTENT is primarily a two-dimensional operation platform. 3D manipulation can be realized by using optical fibres coated with photothermal layers. Nevertheless, we propose that, with its low-power and non-invasive operation, diverse options in the trapping wavelength, and generality in size, shape, and composition of the trapped nanoparticles, OTENT will become a powerful tool in colloid science, life sciences and nanotechnology.

Methods

Materials preparation

The thermoplasmonic substrates were prepared by depositing Au thin films on glass slides (Denton thermal evaporator, base pressure: 9×10^{-6} Torr), followed by thermal annealing at 550 °C in air for 2 hours. Two different thicknesses of Au films were deposited, 4.5 nm and 6.5 nm, which were used for excitation with the 532 nm laser and 660 nm laser, respectively. The 200 nm AuNSs, 100 nm AuNSs (in PBS, 0.1 mM) and AuNRs with nominal absorption peak at 700 nm were purchased from Sigma–Aldrich. The 100 nm AgNSs with citrate-functionalized surfaces were purchased from nanoComposix. The nanoparticle suspension was centrifuged for 5 min (4500 rpm) and re-dispersed in CTAC solutions with the desired concentration. AuNTs in 10 mM CTAC solution were prepared using previously reported synthesis protocols[37]. Silver nanowires were synthesized using the polyol method, according to a procedure reported elsewhere[38]. At the end of the synthesis, silver nanowires were purified through multiple centrifugation steps in acetone and ethanol. Following purification, the final product was dispersed in ethanol for storage. The nanowire suspensions were diluted with CTAC solution to the targeted concentration for trapping experiments.

Optical setup

A 532 nm diode-pumped solid-state laser was expanded with a 5× beam expander and projected onto a DMD. The optical images were created by the DMD and focused onto the thermoplasmonic substrate for optical heating. The size of the beam was reduced by 200 times after being relayed by a 1000 mm doublet lens, a 200 mm doublet lens, an infinity-corrected tube lens and a 40× objective (Nikon, NA 0.75) in a Nikon inverted microscope. For *in-situ* spectroscopy in Fig. 3, the DMD was removed from the optics and a 100× oil objective (Nikon, NA 0.5-1.3) was used to focus the laser beam and to record the scattering signal. An oil condenser (NA 1.43-1.20) was used to focus the incident white light onto the

sample from the top. Trapping and spectroscopy of AuNTs and AuNRs in Figs. 3d and e were achieved with the 532 nm laser. For the single-particle scattering spectra of both AgNSs and AuNSs (Figs. 3b and c), the particles were trapped by a 660 nm laser (without DMD), with a 650 nm shortpass filter inserted between the objective and the spectrometer to block the laser beam. For the imaging of parallel trapping of both AgNSs and AuNTs in Fig. 4, an air condenser (NA 0.95-0.8) was used to focus the white light. A linear visible polarizer (Thorlabs) was inserted between the white light source and the condenser to control the incident light polarization for the dark-field imaging of AgNWs.

In-situ spectroscopy

The scattering signal from the trapped metal nanoparticles was directed to a two-dimensional detector in a spectrometer (Andor). Either the 500 nm grating or 860 nm grating was used for detection, depending on the spectral location of the trapped particles. Reference spectra were recorded when the trapped particles were released from the laser spots and the laser was on. The reference spectra were subtracted to get the scattering signal of the trapped particles. The spectra were finally normalized with the light source spectra.

Computational fluid dynamic simulations

The finite elements method (COMSOL Multiphysics) was used to simulate both the temperature gradient distribution and temperature distribution around the laser beam focused at the substrate-solution interface. A two-dimensional axisymmetric model comprised of a glass substrate, an Au thin film, and solvent was built. Both the pre-defined conjugate heat transfer and laminar flow models were used to include the heat transfer in solids and fluids. A Gaussian-distributed heating source was placed at the substrate-solution interface to model the optical heating from the laser beam. Room temperature was set at all other boundaries.

Finite-difference time-domain (FDTD) simulations

We simulated the electromagnetic field enhancement distribution and the scattering spectra of plasmonic nanoparticles using FDTD methods (Lumerical FDTD). A refractive index of 1.33 was set for the water environment. A mesh size of 1 nm was applied to define the metal nanoparticles. The electric field distribution was recorded by excitation at the resonant wavelength of the LSPs.

Quantifying trapping stiffness

Measurements to quantify the trapping stiffness of trapped AuNSs and AgNSs at varying CTAC concentrations were performed on a previously described custom-built photonic force microscope[39]. In brief, the beam of a 1064 nm laser (Mephisto 500 mW, Coherent, CA, USA) at very low power was expanded and focused through a water immersion objective lens (UPlanSApo 60×W, Olympus, Tokyo, Japan) into the sample chamber. An additional 671 nm laser (Laserglow, Toronto, ON, Canada) was also expanded and coupled into the sample *via* steering mirrors (Cambridge Technology, Bedford, MA, USA) and the same objective lens. The latter was used to achieve trapping at a power of 0.4 mW, while the near-infrared laser with a low power of 25 μW was used to track the confined Brownian motion of

the particle, *via* back-focal plane interferometry. Briefly, forward scattered light from the nanosphere, together with unscattered light of the tracking beam was collected by a condenser lens and projected onto a quadrant photodiode (G6849, Hamamatsu Corporation, NJ, USA), where the two waves interfered. The voltage outputs of the diode's quadrants were amplified by custom-built low noise differential amplifiers (SA500, Oeffner MSR, Plankstadt, Germany) and recorded at 1 MHz bandwidth and 100 kHz sampling frequency. To find the trapping stiffness, we calculated the autocorrelation time τ for 2-5 second time traces, which together with the drag coefficient γ, given by the viscosity of the CTAC solution, and an estimate of the bead's distance to the lower substrate, is related to the trapping stiffness $\kappa_{x,y} = \frac{\gamma}{\tau_{x,y}}$[40].

Data availability

The data that support the plots within this paper and other findings of this study are available from the corresponding author upon reasonable request.

Supplementary Material

Refer to Web version on PubMed Central for supplementary material.

Acknowledgments

The authors acknowledge the financial supports of the Beckman Young Investigator Program, the Army Research Office (W911NF-17-1-0561), the National Aeronautics and Space Administration Early Career Faculty Award (80NSSC17K0520), and the National Institute of General Medical Sciences of the National Institutes of Health (DP2GM128446). We also thank the Texas Advanced Computing Centre at The University of Texas at Austin for providing HPC resources that have contributed to the research results reported within this paper. URL: http://www.tacc.utexas.edu.

References

1. Lehmuskero A, et al. Laser trapping of colloidal metal nanoparticles. ACS Nano. 2015; 9:3453–3469. [PubMed: 25808609]
2. Li Z, Mao W, Devadas MS, Hartland GV. Absorption spectroscopy of single optically trapped gold nanorods. Nano Lett. 2015; 15:7731–7735. [PubMed: 26495877]
3. Selhuber-Unkel C, et al. Quantitative optical trapping of single gold nanorods. Nano Lett. 2008; 8:2998–3003. [PubMed: 18720978]
4. Bosanac L, Aabo T, Bendix PM, Oddershede LB. Efficient optical trapping and visualization of silver nanoparticles. Nano Lett. 2008; 8:1486–1491. [PubMed: 18386911]
5. Pelton M, et al. Optical trapping and alignment of single gold nanorods by using plasmon resonances. Opt Lett. 2006; 31:2075–2077. [PubMed: 16770437]
6. Hansen PM, Bhatia VK, Harrit N, Oddershede L. Expanding the optical trapping range of gold nanoparticles. Nano Lett. 2005; 5:1937–1942. [PubMed: 16218713]
7. Yan Z, Sajjan M, Scherer NF. Fabrication of a material assembly of silver nanoparticles using the phase gradients of optical tweezers. Phys Rev Lett. 2015; 114:143901. [PubMed: 25910124]
8. Bendix PM, Jauffred L, Norregaard K, Oddershede LB. Optical trapping of nanoparticles and quantum dots. IEEE J Sel Top Quantum Electron. 2014; 20:15–26.
9. Ruijgrok PV, et al. Brownian fluctuations and heating of an optically aligned gold nanorod. Phys Rev Lett. 2011; 107:037401. [PubMed: 21838403]
10. Shao L, et al. Gold nanorod rotary motors driven by resonant light scattering. ACS Nano. 2015; 9:12542–12551. [PubMed: 26564095]

11. Min C, et al. Focused plasmonic trapping of metallic particles. Nat Commun. 2013; 4
12. Babynina A, et al. Bending gold nanorods with light. Nano Lett. 2016; 16:6485–6490. [PubMed: 27598653]
13. Govorov AO, Richardson HH. Generating heat with metal nanoparticles. Nano Today. 2007; 2:30–38.
14. Baffou G, Quidant R. Thermo-plasmonics: Using metallic nanostructures as nano-sources of heat. Laser Photonics Rev. 2013; 7:171–187.
15. Ndukaife JC, et al. Long-range and rapid transport of individual nano-objects by a hybrid electrothermoplasmonic nanotweezer. Nat Nanotechnol. 2016; 11:53–59. [PubMed: 26524398]
16. Braun M, Cichos F. Optically controlled thermophoretic trapping of single nano-objects. ACS Nano. 2013; 7:11200–11208. [PubMed: 24215133]
17. Braun M, et al. Single molecules trapped by dynamic inhomogeneous temperature fields. Nano Lett. 2015; 15:5499–5505. [PubMed: 26161841]
18. Flores-Flores E, et al. Trapping and manipulation of microparticles using laser-induced convection currents and photophoresis. Biomed Opt Express. 2015; 6:4079–4087. [PubMed: 26504655]
19. Chen J, et al. Thermal gradient induced tweezers for the manipulation of particles and cells. Sci Rep. 2016; 6:35814. [PubMed: 27853191]
20. Lin L, et al. Light-directed reversible assembly of plasmonic nanoparticles using plasmon-enhanced thermophoresis. ACS Nano. 2016; 10:9659–9668.
21. Nikoobakht B, El-Sayed MA. Evidence for bilayer assembly of cationic surfactants on the surface of gold nanorods. Langmuir. 2001; 17:6368–6374.
22. Smith DK, Korgel BA. The importance of the CTAB surfactant on the colloidal seed-mediated synthesis of gold nanorods. Langmuir. 2008; 24:644–649. [PubMed: 18184021]
23. Tadros, TF. Applied surfactants: Principles and applications. Vol. Ch. 3. Wiley-VCH Verlag GmbH & Co. KGaA; Weinheim: 2005.
24. Reichl M, Herzog M, Götz A, Braun D. Why charged molecules move across a temperature gradient: the role of electric fields. Phys Rev Lett. 2014; 112:198101. [PubMed: 24877967]
25. Majee A, Würger A. Charging of heated colloidal particles using the electrolyte seebeck effect. Phys Rev Lett. 2012; 108:118301. [PubMed: 22540514]
26. Zheng Y, et al. Nano-optical conveyor belt, part II: demonstration of handoff between near-field optical traps. Nano Lett. 2014; 14:2971–2976. [PubMed: 24807058]
27. Grigorenko AN, Roberts NW, Dickinson MR, Zhang Y. Nanometric optical tweezers based on nanostructured substrates. Nat Photonics. 2008; 2:365–370.
28. Amos DA, Markels JH, Lynn S, Radke CJ. Osmotic pressure and interparticle interactions in ionic micellar surfactant solutions. J Phys Chem B. 1998; 102:2739–2753.
29. Vigolo D, Buzzaccaro S, Piazza R. Thermophoresis and thermoelectricity in surfactant solutions. Langmuir. 2010; 26:7792–7801. [PubMed: 20146491]
30. Würger A. Hydrodynamic boundary effects on thermophoresis of confined colloids. Phys Rev Lett. 2016; 116:138302. [PubMed: 27082005]
31. Prikulis J, et al. Optical spectroscopy of single trapped metal nanoparticles in solution. Nano Lett. 2004; 4:115–118.
32. Demergis V, Florin EL. Ultrastrong optical binding of metallic nanoparticles. Nano Lett. 2012; 12:5756–5760. [PubMed: 23035835]
33. Iracki TD, Beltran-Villegas DJ, Eichmann SL, Bevan MA. Charged micelle depletion attraction and interfacial colloidal phase behavior. Langmuir. 2010; 26:18710–18717. [PubMed: 21077612]
34. Ohlinger A, Nedev S, Lutich AA, Feldmann J. Optothermal escape of plasmonically coupled silver nanoparticles from a three-dimensional optical trap. Nano Lett. 2011; 11:1770–1774. [PubMed: 21410159]
35. Tong L, Miljković VD, Johansson P, Käll M. Plasmon hybridization reveals the interaction between individual colloidal gold nanoparticles confined in an optical potential well. Nano Lett. 2011; 11:4505–4508. [PubMed: 21142200]
36. Blattmann M, Rohrbach A. Plasmonic coupling dynamics of silver nanoparticles in an optical trap. Nano Lett. 2015; 15:7816–7821. [PubMed: 26605492]

37. Scarabelli L, et al. Monodisperse gold nanotriangles: size control, large-scale self-assembly, and performance in surface-enhanced Raman scattering. ACS Nano. 2014; 8:5833–5842. [PubMed: 24848669]

38. Coskun S, Aksoy B, Unalan HE. Polyol synthesis of silver nanowires: an extensive parametric study. Cryst Growth Des. 2011; 11:4963–4969.

39. Bartsch TF, et al. Nanoscopic imaging of thick heterogeneous soft-matter structures in aqueous solution. Nat Commun. 2016; 7:12729. [PubMed: 27596919]

40. Pralle A, Florin EL, Stelzer EHK, Hörber JKH. Local viscosity probed by photonic force microscopy. Applied Physics A. 1998; 66:S71–S73.

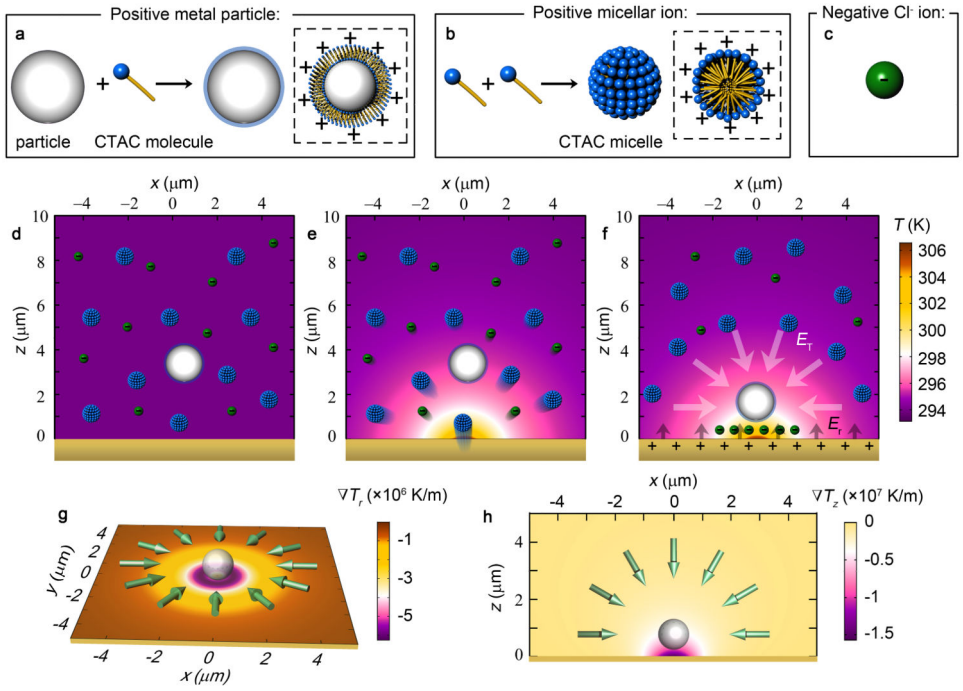

Figure 1. Working principle of OTENT

a, Surface charge modification of a metal nanoparticle by CTAC adsorption. **b,** Formation of CTAC micelles. **c,** Schematic view of a Cl^- ion. **d,** Dispersion of a single metal particle and multiple ions in the solution without optical heating. **e,** Thermophoretic migration of the ions under optical heating. **f,** Steady ionic distribution under optical heating generates a thermoelectric field E_T for trapping the metal nanoparticle. The repulsive electric field E_r arises from the positive charge of the thermoplasmoic substrate and balances E_T. **g,** Simulated in-plane temperature gradient and direction of the corresponding trapping force. **h,** Simulated out-of-plane temperature gradient and direction of the corresponding trapping force. The incident laser beam in (**e-h**) has a diameter of 2 μm and an optical power of 0.216 mW. The green arrows in (**g, h**) show the direction of the trapping force.

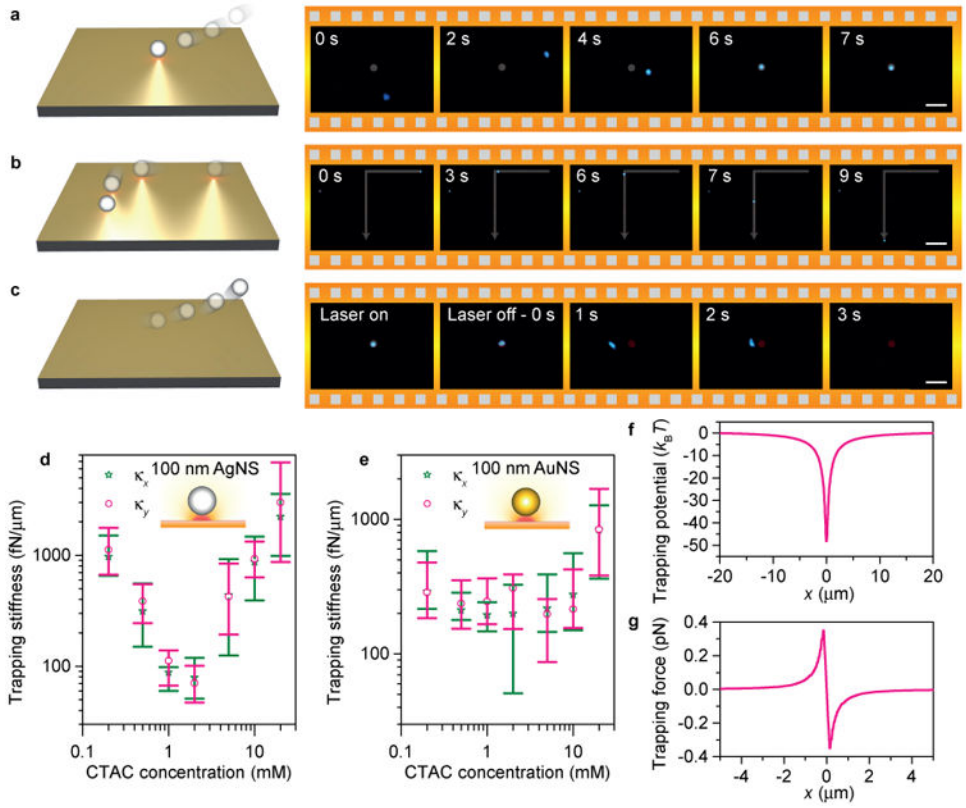

Figure 2. Single-nanoparticle trapping and manipulation

Schematic illustration and successive optical images showing **a,** trapping **b,** dynamic manipulation, and **c,** release of a single 100 nm AgNS. The grey disks and the red disks mean that the laser is turned on or turned off, respectively. The grey lines show the manipulation trajectory of the trapped AgNS. Measured trapping stiffness of single **d,** 100 nm AgNSs and **e,** 100 nm AuNSs as a function of CTAC concentration. κ_x and κ_y are the trapping stiffness along x and y axis, respectively. The error bars show the deviation in multiple measurements with different particles. **f,** Trapping potential and **g,** trapping force of a single 100 nm AgNS at CTAC concentration of 20 mM. The laser has a wavelength of 671 nm and an optical power of 0.4 mW in **d**-**g**. Scale bars: 10 μm (**a, c**) and 20μm (**b**).

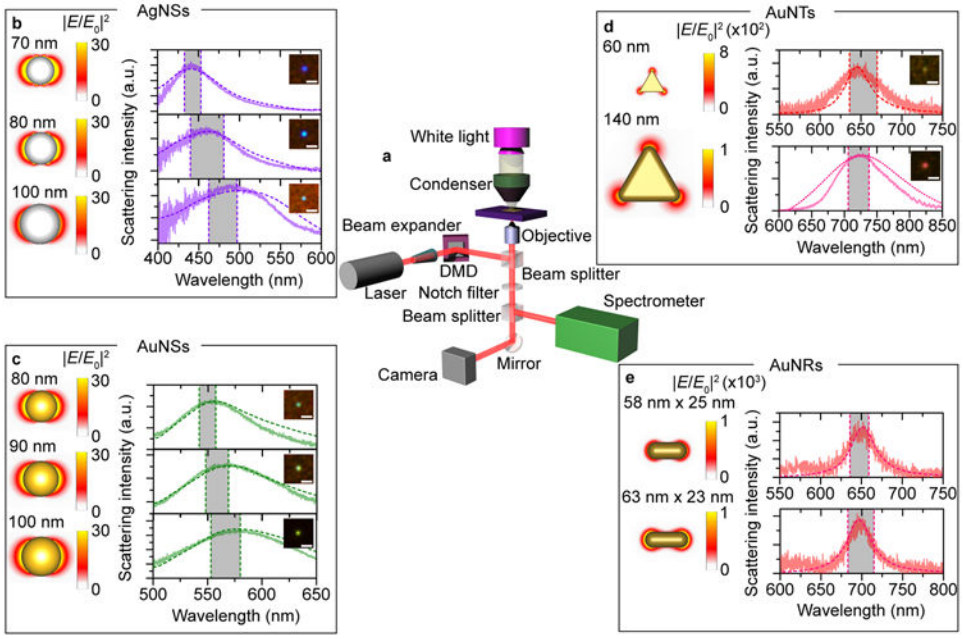

Figure 3. *In-situ* optical spectroscopy of different metal nanoparticles trapped *via* OTENT

a, Optical setup of OTENT with *in-situ* dark-field optical imaging and spectroscopy. Dark-field optical images, experimental and simulated scattering spectra, and electric field profiles of single AgNSs **b,** with diameters of 70, 90 and 100 nm; single AuNSs **c,** with diameters of 80, 90 and 100 nm; single AuNTs **d,** with side lengths of 60 and 140 nm; single AuNRs **e,** with lengths of 50-60 and diameters of 19-25 nm and corresponding absorption peaks at around 650 nm (top panel); with lengths of 63-73 nm and diameters of 19-25 nm and corresponding absorption peaks at around 700 nm (bottom panel). The solid and dashed curves represent experimental and simulated scattering spectra, respectively. The grey rectangles represent the peak distributions recorded in multiple experiments. Scale bars: 2 μm.

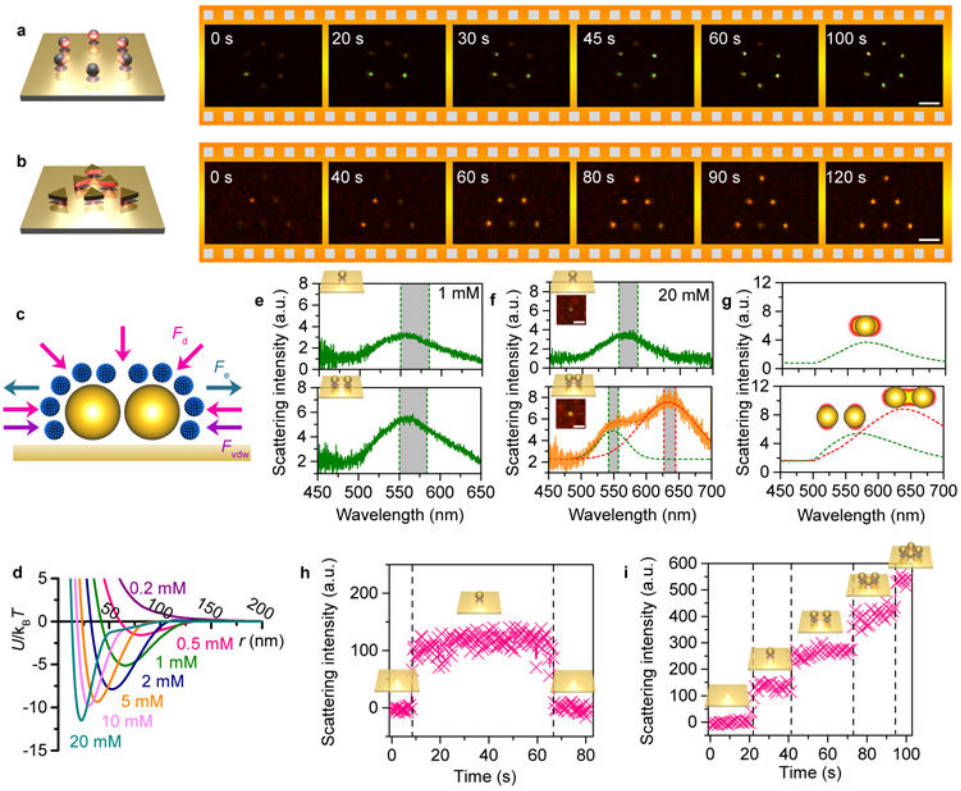

Figure 4. Parallel and multiple trapping *via* OTENT

Parallel trapping of **a,** six 100 nm AgNSs into a circular pattern, and **b,** six 140 nm AuNTs into a triangular pattern. **c,** Interaction forces between two trapped nanoparticles. **d,** Calculated interaction potential between two AuNSs at different CTAC concentrations. Scattering spectra of a single AuNS (top) and two AuNSs (bottom) in **e,** 1 mM and **f,** 20 mM CTAC solution. **g,** Simulated scattering spectra of a single AuNS (top) and two AuNSs (bottom) in 20 mM CTAC solution. The red and green dashed curve represent the longitudinal and transverse plasmon mode, respectively (**f** and **g**). Trapping dynamics of **h,** a single AuNS and **i,** multiple AuNSs in 1 mM CTAC solution. The grey rectangles represent the peak distributions recorded in multiple experiments. The particle diameter is 100 nm in **d-i**. Scale bars: 5μm (**a, b**) and 2 μm (**f**).